Study on the effect of two-phase fuel on the detonation-wave collision process in a rotating detonation ramjet engine

Xixuan Huang, Zhiyong Lin*
School of Aeronautics and Astronautics, Sun Yat-sen University,
No. 66, Gongchang Road, Guangming District,
Shenzhen, Guangdong 518107, P.R. China

1 Introduction

Detonation wave (DW) collision is a typical phenomenon in rotating detonation engines(RDE). Lin [1,2] reported an unstable DW collision phenomenon in RDE experiments utilizing hydrogen and methane as the fuels, respectively. Through pressure monitoring, Xie [3] and Lin [2] found in their RDE experiments that the collision of two DWs generated a local pressure increase as well as the decay and re-initiation of the pressure peak. According to Bluemner's research [4], the propagation mode of DWs changes as reactive mass flow increases. First, the DW switches from equal to unequal double wave collisions, then to single explosion waves colliding with multiple counter-propagating wave elements, and finally to single wave operating in a stable mode. Through numerical simulation, Xia [5,6] investigated the double wave collision structure and mode transition of the DW propagation mode in the hollow combustor.

There have been some researches on the mechanism of DW collision. Ng [7] Firstly studied the mechanism of DW collision phenomenon by one-dimensional theoretical analysis and numerical simulation. Through an experiment, Zhu et al. [8] created the collision of a DW and a shock wave and determined the cell structure that resulted from the collision using a smoked foil. Since the flow directed by the incident shock wave is opposite to the flow led by the DW, the transmitted DW initially decouples, the chemical reaction rate behind DW slows down, and the thickness of flame increases. The incomplete-conbustion products and complete-combustion products mix and create local explosion waves in the high-temperature, high-pressure region where the two waves both passed through, and the transmitted DW swiftly transforms into overdrive detonation. After a moment, it transforms into a CJ detonation and starts to spread steadily. Zhang et al. [9] found that for incident shock waves with moderate intensity (shock wave propagating at speed of Mach number 1.5 and 2.0, respectively), the decoupling effect between combustion surface and DW is very significant. The dominant factor in this case is that the flow behind the shock wave that is reverse to DW moving direction leads to a decrease in the chemical reaction rate behind the transmitted DW, and the shock wave has a weak effect on the temperature and pressure of the mixture behind the transmitted DW, which is taken as case 1. However, the chemical reaction zone behind the transmitted DW is less influenced when the intensity of the incident shock wave is low (shock wave propagating at speed of Mach number 1.2) or high (shock wave propagating at speed of Mach number 3.0). This is because the post-collision state is greatly determined by two factors: the first is the promotion effect of the high temperature caused by the shock wave on the chemical reaction, and

Correspondence to: linzhiyong@mail.sysu.edu.cn

the second is the suppression effect of the convective expansion following the collision on the chemical reaction of the DW. Under the condition where the intensity of shock wave is low, the opposite effect of the second factor plays a dominant role, and the post-wave flow behind transmitted DW is less affected, so the inhibition effect on chemical reaction is less, which is regarded as case 2. Under the condition where the intensity of shock wave is high, although the convective expansion effect is stronger, it also improves the thermodynamic state of combustible mixture and induces stronger activation reaction, so that the chemical reaction after transmitted DW is quickly established, the first factor plays a dominant role, which is considered as case 3.

The DW collision phenomenon frequently occurs in practical rotating detonation ramjet engines(RDRE) operating at high Mach numbers [10]. When adding liquid kerosene as fuel, the movement and evaporation of the fuel will change the gas state and fuel distribution in the combustor, which will alter the DW propagation characteristics [11]. However, there is currently a lack of knowledge regarding how two-phase fuel affects the DW collision characteristics. In this article, under the condition of incoming flow of mach number M=6, the effect of two-phase fuel on DW collision characteristics is investigated.

2 Governing equations and computational method

It is necessary to consider the gas phase and the liquid phase and their interaction process in the calculation of rotating detonation. In this paper, the gas phase is considered as the continuous phase and the liquid phase is considered as the discrete phase. The governing equation will be used to describe the gas phase and the liquid phase respectively.

2.1 Governing equations for gas phase

The control equations for the compressible reacting flow consist of the mass conservation equation, the momentum conservation equation, the energy conservation equation, and the species transport equation. The ideal gas equation is used to close the set of the control equations.

$$\frac{\partial \rho_g}{\partial t} + \frac{\partial}{\partial x_j}\left(\rho_g u_j\right) = S_m \tag{1}$$

$$\frac{\partial}{\partial t}\left(\rho_g u_i\right) + \frac{\partial}{\partial x_j}\left(\rho_g u_i u_j + P\delta_{ij} - \tau_{ij}\right) = S_{F,i} \tag{2}$$

$$\frac{\partial}{\partial t}\left(\rho_g e_t\right) + \frac{\partial}{\partial x_j}\left(\left(\rho_g e_t + p\right) u_j - u_i \tau_{ij} - q_j\right) = S_Q \tag{3}$$

$$\frac{\partial}{\partial t}\left(\rho_g Y_k\right) + \frac{\partial}{\partial x_j}\left(\rho_g Y_k u_j\right) + \nabla\left(-D\nabla\left(\rho_g Y_k\right)\right) = S_{\text{combustion, } k} + S_{Y_k} \tag{4}$$

$$p = \rho_g R T_g \tag{5}$$

ρ_g is the density of the gas phase, u_i is the velocity component in the i direction, T_g is the static temperature of the gas, p is the static pressure, R is the universal gas constant, Y_k is the mass fraction of component k, τ_{ij} is Newtonian viscous stress tensor, e_t refers to the total energy, and the chemical reaction source is calculated using a finite rate combustion model. The terms S_m , S_F and S_Q on the right side of the 1, 2 and 3 equations represent the increase in gaseous fuel mass source term caused by liquid evaporation, gaseous phase, momentum exchange between the liquid phases due to interface drag force and energy changes in the gas phase due to evaporation of the liquid phase.

The model consists of the following transport equations for k and ϵ:

$$\frac{\partial(\rho_g k)}{\partial t} + \frac{\partial}{\partial x_j}\left(u_j \rho_g k\right) = \frac{\partial}{\partial x_j}\left[\left(\mu + \frac{\mu_t}{\sigma_k}\right)\frac{\partial k}{\partial x_j}\right] + P_k - \rho_g \epsilon \tag{6}$$

$$\frac{\partial(\rho_g \epsilon)}{\partial t} + \frac{\partial}{\partial x_j}\left(u_j \rho_g \epsilon\right) = \frac{\partial}{\partial x_j}\left[\left(\mu + \frac{\mu_t}{\sigma_\epsilon}\right)\frac{\partial \epsilon}{\partial x_j}\right] + \left(C_{\epsilon 1} P_k - C_{\epsilon 2}\rho_g \epsilon + E\right) T_t^{-1} \tag{7}$$

in which the rate of production of turbulence energy P_k is expressed as $P_k = -\rho_g \overline{u_i u_j}\partial u_i/\partial x_j$, T_t refers to realizable estimate of the turbulence timescale,

$$T_t = \frac{k}{\epsilon}\max\left\{1, \zeta^{-1}\right\}, \quad \zeta = \sqrt{R_t/2} \tag{8}$$

and the turbulence Reynolds number R_t is defined as $\rho_g k^2/(\mu\epsilon)$. The model constants are given by

$C_\mu = 0.09, C_{\epsilon 1} = 1.44, C_{\epsilon 2} = 1.92, \sigma_k = 1.0, \sigma_\epsilon = 1.3$

The eddy viscosity, μ_t, is obtained from

$$\begin{aligned} \mu_t &= \min\left\{C_\mu f_\mu \rho_g k^2/\epsilon, \phi\frac{\rho k}{S}\right\} \\ \phi &= \begin{cases} 2/3, & \text{Schwartz} \\ 0.31, & \text{Bradshaw} \end{cases} \end{aligned} \tag{9}$$

where $S = \sqrt{S_{kl}S_{kl}/2}$ is the dimensional strain magnitude and f_μ is a low-Reynolds number function

$$f_\mu = \frac{1 - \exp^{-0.01 R_t}}{1 - \exp^{-\sqrt{Rt}}}\max\left\{1, \left(\frac{2}{R_t}\right)^{\frac{1}{2}}\right\} \tag{10}$$

2.2 Governing equations for liquid phase

The Euler dispersed phase method is used to describe the liquid phase (discrete phase), and the governing equations also include mass conservation equations, momentum conservation equations, and energy equations

$$\frac{\partial\left(\rho_p\right)}{\partial t} + \nabla\cdot\left(\rho_p \vec{u}_p\right) = \dot{m} = -S_m \tag{11}$$

$$\frac{\partial\left(\rho_p \vec{u}_p\right)}{\partial t} + \nabla\cdot\left(\rho_p \vec{u}_p \vec{u}_p\right) = \vec{F}_D + \vec{F}_{T,D} + \dot{m}\vec{u}_p = -S_F \tag{12}$$

$$\frac{\partial\left(\rho_p e_p^0\right)}{\partial t} + \nabla\cdot\left(\rho_p e_p^0 \vec{u}_p\right) = \dot{Q}_p + \dot{m}\left(e_p^0 + L_v\left(T_p\right)\right) = -S_{Q,p} \tag{13}$$

Here, ρ_p is "fluidized" density of fuel particle, $\vec{u}_p$ is the velocity vector of the liquid component, $\dot{m}$ is rate of production of mass for particle,$\vec{F}_D$ is the interphase drag force, $\vec{F}_{T,D}$ is the turbulent dispersion force, $\dot{Q}_p$ is the power of heat conduction between gas and liquid per unit volume, e_p^0 is the internal energy in the liquid phase, $L_v\left(T_p\right)$ is the latent heat of evaporation in the liquid phase.

In addition, it is necessary to supplement the liquid particle number density equation

$$\frac{\partial N}{\partial t} + \nabla \cdot (N\vec{u}_p) = 0 \tag{14}$$

N is the number of liquid particles per unit volume, "fluidized" density ρ_p is determined by solving the number density equation.

Interphase drag force is expressed by the following formula

$$\mathbf{F}_D = m_p \frac{18\mu}{\rho_p d_p^2} \frac{C_D R_e}{24} \left(\vec{u_g} - \vec{u_p}\right) \tag{15}$$

Where, d_p is the diameter of liquid particle, R_e is the relative Reynolds number, and $C_d$is the drag coefficient, which are calculated by the equations 16 and 17 respectively

$$\mathrm{Re} = \frac{\rho d_p \left|\bar{u}_p - \bar{u}\right|}{\mu} \tag{16}$$

$$C_D = \begin{cases} \frac{24}{Re} \text{ if } \mathrm{Re} < 1 \\ \frac{24}{Re_p}\left(1 + 0.15 Re_p^{0.687}\right) \text{ if } 1 \le \mathrm{Re}_p \le 1000 \\ 0.44 \quad \text{if } \mathrm{Re}_p > 1000 \end{cases} \tag{17}$$

The turbulent dispersion force is expressed as

$$\frac{\vec{F}_{T\cdot D}}{\rho_p} = -\frac{f_D}{\tau_u} \frac{\nu_t}{\mathrm{Pr}_t} \left(\frac{\nabla \eta_p}{\eta_p} - \frac{\nabla \eta_g}{\eta_g}\right) \tag{18}$$

Wherein, ν_t is the eddy dynamic viscosity, Pr_t is the turbulent Prandtl number, η_p and η_g are the volume fractions of the liquid and gas phases in the space, respectively.

The phase change source term is expressed as

$$\dot{m} = N\rho_p \left(4\pi r\right) \left(r \frac{dr}{dt}\right) \tag{19}$$

Among them, r is the liquid particle diameter. Using the boiling-Hertz-Knudsen evaporation model, the droplet diameter change is calculated by the following formula

$$r\frac{dr}{dt} = -\alpha_v \frac{r}{\rho_p} \sqrt{\frac{1}{2\pi R_p}} \left(\frac{p_{sat}}{\sqrt{T_p}} - \frac{p}{\sqrt{T_g}}\right) \tag{20}$$

α_v is the evaporation constant, R_p is the gas constant of the liquid component vapor, p_{sat} is the saturated vapor pressure of the liquid phase, calculated by the formula 21

$$\frac{p_{sat}}{p_{sat,ref}} = \exp\left[\frac{-L_V}{R_p}\left(\frac{1}{T_p} - \frac{1}{T_p^{evap}}\right)\right] \tag{21}$$

$p_{sat,ref}$ is the saturated vapor pressure at the evaporation temperature.

3 Computational Model and designed cases

The designed engine model whose dimension was inspired by real rotating detonation engine is shown in Figure1(a). The inner diameter of the engine isolator is 140 mm with the width of the annular channel of 10 mm, the inner diameter of the combustor is 130mm with the width of the annular channel of 20 mm. At the entrance of the combustor, 18 struts evenly distributed among the circumferential direction are used for injection, wherein the diameter of the struts is 2 mm, and each strut is provided with 4 tangential injection holes with a diameter of 0.4mm. Three cylindrical supporting blocks(SUBL) are evenly arranged among the azimuthal direction near the outlet of the combustor, and the diameter of the blocking block is 36mm, producing cross section's maximum blockage ratio of 0.23. The combustor and the far field are connected by a plug nozzle. Here, the far field diameter is 0.37 m.

It has been obtained in the author's study [10] that under the condition of Mach number M=6 inflow, the design configuration is dual DWs collision mode, as depicted in the Figure1(b). Therefore, based on this result, two-phase fuel conditions are added to study the role of two-phase fuel in DW collision process. Gas-phase fuel case is named M6-sp, two-phase case is named M6-tp, incoming air condition and fuel injection condition are shown in Table 1 and Table 2.

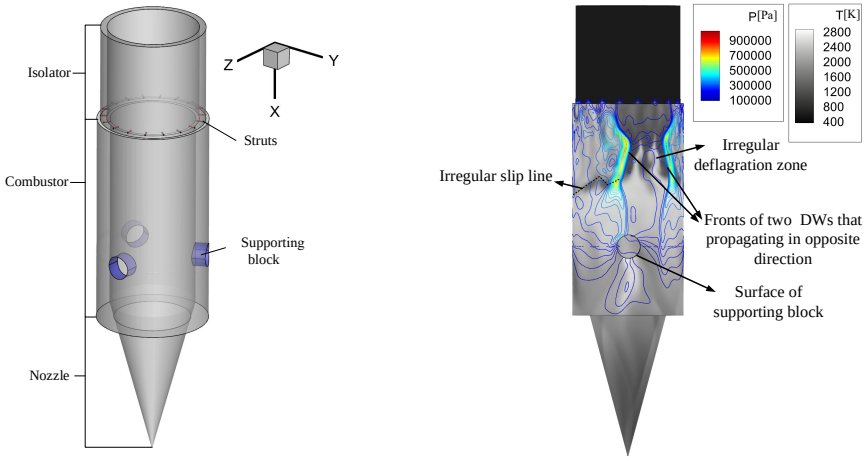

(a) RDRE configuration with three cylindrical SUBLs in combustor and struts for fuel injection

(b) Collision structure of two DWs with incoming flow at speed of Mach number 6

Figure 1: Wave structure of two DWs collision in designed configuration, the two waves move in opposing directions

Table 1: Incoming air conditions

	Total Temperature /K	Total pressure /MPa	Total pressure recovery coefficient	Entrance Mach number of isolator
M6-sp/M6-tp	1640	3.8	0.3	3

Table 2: Single-phase and two-phase fuel injection conditions

	Total injection pressure/MPa	Equivalence ratio	Liquid fuel mass fraction	Liquid fuel droplet diameter/micron
M6-sp	1.8	0.8071		
M6-tp	1.8	0.8789	13.09%	20

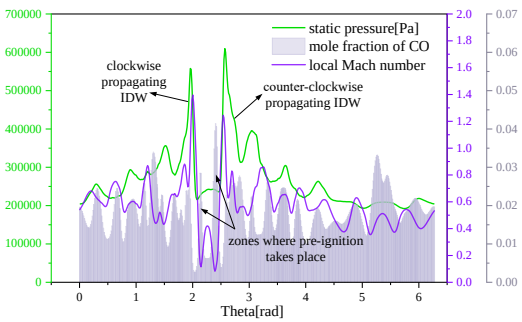

(a) One-dimensional flow structure before DW collision of M6-sp

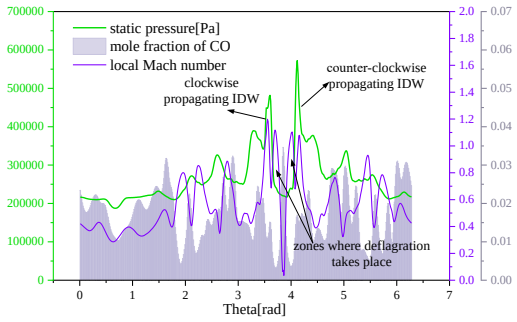

(b) One-dimensional flow structure before DW collision of M6-tp

Figure 2: One-dimensional flow structure before DW collision for Mach 6 cases: static pressure, local Mach number and CO mole fraction distribution in the circumferential direction passing the detonation wave pressure peak

4 Results

4.1 One-dimensional DWs structure

The one-dimensional structure diagram of two DWs corresponding to case M6-sp and case M6-tp is drawn in Figure 2(a) and Figure 2(b). First, it is discovered that the two DWs' intensities differ. The DW propagating clockwise is weaker than the DW moving counterclockwise. For case M6-sp, there is a considerable concentration of carbon monoxide in the upstream area of the DW, which is an byproduct of incomplete kerosene combustion , indicating that the pre-combustion effect of upstream region of the DW is more prominant. For case M6-tp, a clear deflagration zone can be seen in the area upstream of the incident DW, which is the area with a high Mach number but a low carbon dioxide mole fraction. In order to further judge the influence of two-phase fuel on the DW collision process, the features before and after the DW collision should be further examined.

4.2 Comparison of propagation speed of DW before and after collision with theoretical propagation speed

Two hypotheses are considered in order to further assess the propagation mode of two DWs collision. The first is to assess the wave speed through the flow condition upstream and downstream of the wave front using the theory of a normal shock wave. The normal shock wave relation states:

$$\frac{p_2}{p_1} = 1 + \frac{2\gamma}{\gamma+1}(M_{n,1}^2 - 1)$$

Where p_1, p_2 denote the static pressure upstream and downstream of the wave, γ denotes the upstream gas' specific heat ratio, and $M_{n,1}$ denotes the gas's relative Mach number to the DW. If the speed of

wave front is known, it is possible to determine the propagation speed of the DW by computing the value of $M_{n,1}$. Based on experiments when a DW encounters an obstruction, the second hypothesis for determining propagation speed was developed. It is described in the literature [15–17] that the detonation experiment is carried out in the pipeline with block obstacles. A fast deflagration, also known as a choked flame or a quasi-steady detonation, is observed in the experiment when a DW collides with block barriers. Besides, it is found that the propagation speed of the DW surface in this state is equivalent to the sound speed of the product behind the wave combustion. According to Bluemner et al. [4], the collision between a detonation wave and an obstruction can be compared to a detonation wave collision. In the experimental results of two-wave collision with different propagation speeds, they discovered that the operating mode of the collision of two waves was in fact connected to the relative propagation speed of the two detonation waves.

It is considered that the DW propagation speed is proportional to its energy. The propagation speed of the clockwise and counterclockwise propagating DWs before and after the collision and the propagation speed estimated by the above theory are plotted in Figure 3. For the counterclockwise propagating DW (strong intensity) in the two cases, before the collision, the propagation speed of DW is greater than or equal to the propagation speed estimated by the shock wave theory, indicating that the detonation wave and the chemical reaction after the wave are strongly coupled and "driven" by the flame. Immediately following the collision, their propagation speed is very close to the sound speed of post-wave combustion product calculated by the choking flame/quasi-steady state detonation theory. This suggests that the decoupling of the flame surface and the detonation surface hardly ever happens after the collision, which means DW persists in a critical state. However, the propagation speed of counterclockwise DW in the next stage after the collision is lower than that before the collision and lower than that estimated by shock wave theory, which means the intensity of counterclockwise DW is weakened due to the collision. DW's decoupling is believed to occur after collision for clockwise moving DWs (weak intensity), as their propagation speed before collision is lower than that predicted by shock wave theory. The propagation speed during the collision is obviously lower than the sound speed of the combustion product after the quasi-steady detonation wave, indicating that the DWs decoupling and re-initiation occurs after collision. The clockwise rotating detonation wave's propagation speed for case M6-sp returns to the pre-collision level following the collision. For case M6-tp, the intensity of the clockwise rotating DW increases following a collision and also higher than that of the counter-clockwise rotating DW at the same time. From the aforementioned phenomenon, it is clear that when DWs collide, energy moves from stronger to weaker DW. The two-wave collision system's overall energy change follows the law of entropy increasing. Since there is energy loss in the system during the two-wave collision, the total intensity of the DW should be lower than it was prior to the collision if there is no external force.

4.3 Two-phase fuel's influence on the DW collision process

When viewed from the perspective of two counterclockwise rotating detonation waves, the decoupling of the flame surface behind the DWs occurs as a result of the collision with medium-intensity shock waves, which is case 1 mentioned above in Zhang's work [9]. The two counterclockwise incident DWs are not decoupled because they are colliding with weak incident shock waves, which causes them to belong to case 2. In the case M6-sp, preignition primarily dominates the uptream zone of incident DW, whereas deflagration primarily dominates the uptream zone of the incident DW in the case M6-tp. The primary distinction between the two cases is whether or not the shared post-wave region of the two DWs during the collision has a core of high thermodynamic state. This core does not exist in case M6-sp because CO formation by preignition is primarily an endothermic process, and reinitiation can only be achieved by hot spots, as shown in Figure 4(a). In case M6-tp, the presence of deflagration wave will form this core, as shown in Figure 4(b). As a result, in case M6-sp, the intensity of the DW

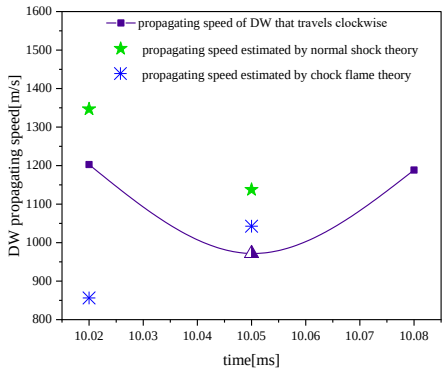

(a) Comparison of the clockwise detonation wave's theoretical and observed propagation speeds before and after collision for M6-sp

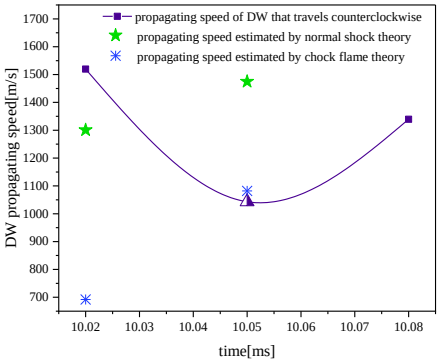

(b) Comparison of the counterclockwise detonation wave's theoretical and observed propagation speeds before and after collision for M6-sp

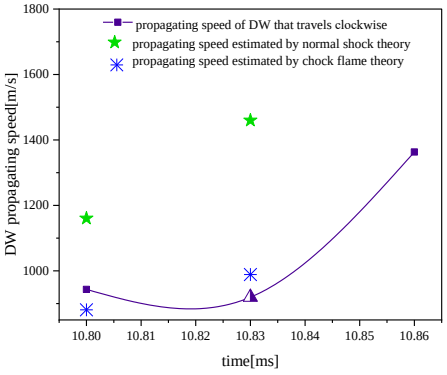

(c) Comparison of the clockwise detonation wave's theoretical and observed propagation speeds before and after collision for M6-tp

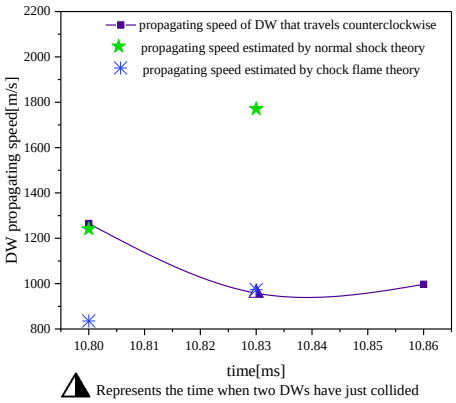

(d) Comparison of the counterclockwise detonation wave's theoretical and observed propagation speeds before and after collision for M6-tp

Figure 3: Comparison of DW propagation speed with that calculated by normal shock wave theory and choked flame model before and after detonation wave collision for Ma6 incoming flow

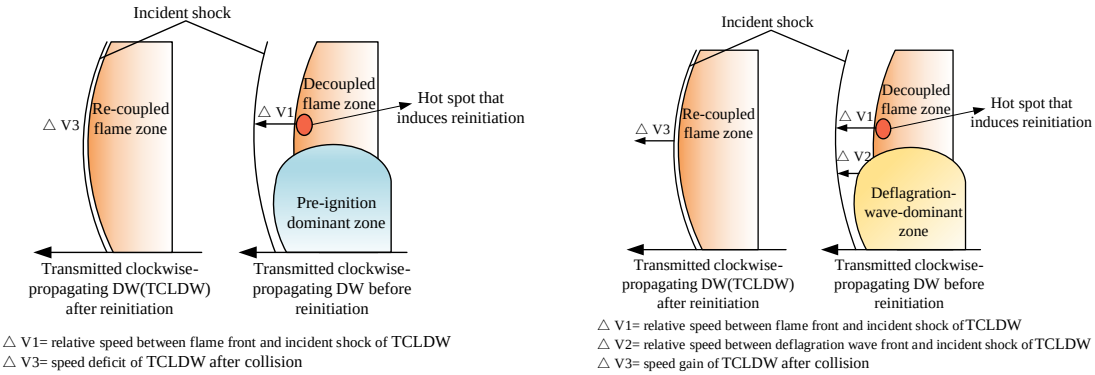

(a) Clockwise detonation wave reinitiation process in M6-sp

(b) Clockwise detonation wave reinitiation process in M6-tp

Figure 4: Reinitiation process for two cases, the gas-phase fuel case is affected by the preignition zone, and the two-phase fuel case is mainly affected by the deflagration zone

propagating counterclockwise decreases noticeably after the collision relative to that before the collision, while the propagation speed of the clockwise DW which obtains the energy only returns to a level that is somewhat similar to that before the collision. Due to the presence of the core, the propagation speed of the counterclockwise propagating DW for the two-phase fuel condition decreases compared to that before the collision, but the propagation speed of the clockwise propagating DW significantly increases compared to that before the collision.

In the two Mach 6 cases, the speed variation rates of the clockwise and counterclockwise DWs with respect to the speed before collision are calculated. The calculation formula is as follows

$$Speed\ change\ ratio = \frac{V_{after\ collision} - V_{before\ collision}}{V_{before\ collision}}$$

Table 3 displays the result. In case M6-sp, where preignition was dominant in upstream area, the collision process results in energy loss for the DW system because there is no external force present, such as a deflagration wave. According to $\Delta V3$ in Figure 4(b), the total change rate of the speed following the detonation collision is positive for case M6-tp, indicating that the deflagration wave plays a role in "boosting" the transmitted wave during the collision. When two waves collide, the deflagration wave in front of the detonation wave can provide a small energy boost to the transmitted detonation wave and lessen energy loss.

Table 3: Speed change ratio of detonation wave before and after collision

	Speed change ratio of clockwise rotating DW after collision	Speed change ratio of counterclockwise rotating DW after collision	Total speed change ratio
M6-sp	-1.18%	-11.85%	-7.14%
M6-tp	44.52%	-21.20%	6.82%

5 conclusion

The process of energy flowing from the stronger detonation wave(DW) to the weaker DW occurs when two waves collide. For the counterclockwise propagating DW (strong intensity) in studied cases, before the collision, the DW and the chemical reaction after the wave are strongly coupled and "driven" by

the flame. Immediately following the collision, the decoupling of the flame surface and the detonation surface hardly ever happens. However, the propagation speed of counterclockwise DW in the next stage after the collision is lower than that before the collision, which means the intensity of counterclockwise DW is weakened due to the collision. DW's decoupling is believed to occur after collision for clockwise moving DWs (weak intensity), as their propagation speed before collision is lower than that predicted by shock wave theory. The propagation speed during the collision is obviously lower than the sound speed of the combustion product after the quasi-steady DW, indicating that the DWs decoupling and re-initiation occurs after collision. The deflagration wave caused by two-phase fuel plays a role of "boosting" the transmitted wave during the collision, giving the transmitted DW a certain energy gain and reducing the energy loss during the collision.

References

[1] Lin, W., Zhou, J., Liu, S., Lin, Z., & Zhuang, F. (2015). Experimental study on propagation mode of H2/Air continuously rotating detonation wave. International Journal of Hydrogen Energy, 40(4), 1980-1993.

[2] Lin, W., Zhou, J., Liu, S., & Lin, Z. (2015). An experimental study on CH4/O2 continuously rotating detonation wave in a hollow combustion chamber. Experimental Thermal and Fluid Science, 62, 122-130.

[3] Xie, Q., Wen, H., Li, W., Ji, Z., Wang, B., & Wolanski, P. (2018). Analysis of operating diagram for H2/Air rotating detonation combustors under lean fuel condition. Energy, 151, 408-419.

[4] Bluemner, R., Bohon, M. D., Paschereit, C. O., & Gutmark, E. J. (2019). Counter-rotating wave mode transition dynamics in an RDC. International Journal of Hydrogen Energy, 44(14), 7628-7641.

[5] Xia, Z., Tang, X., Luan, M., Zhang, S., Ma, Z., & Wang, J. (2018). Numerical investigation of two-wave collision and wave structure evolution of rotating detonation engine with hollow combustor. International Journal of Hydrogen Energy, 43(46), 21582-21591.

[6] Xia, Z. J., Luan, M. Y., Liu, X. Y., & Wang, J. P. (2020). Numerical simulation of wave mode transition in rotating detonation engine with OpenFOAM. International Journal of Hydrogen Energy, 45(38), 19989-19995.

[7] Ng, H. D., Nikiforakis, N., & Lee, J. H. S. (2005). Head-on collision of a detonation with a planar shock wave. In Shock Waves: Proceedings of the 24th International Symposium on Shock Waves Beijing, China July 11–16, 2004 (pp. 745-750). Springer Berlin Heidelberg.

[8] Yu-Jian, Z. H. U. (2008). An experimental study on head-on collision of detonation with shock. Chinese Journal of Theoretical and Applied Mechanics, 40(6), 721-728.

[9] Han, G., Jiang, Z., & Zhang, D. (2008). Numerical investigation on the collision between detonations and shocks. Chinese Journal of Theoretical and Applied Mechanics, 40(2), 154-161.

[10] Huang, X., Lin, Z., Liu, Y., & Wu, Q. (2022). Numerical simulation on the operating characteristics of rotating detonation ramjet engines at high flight mach number. International Journal of Hydrogen Energy.

[11] Ren, Z., & Zheng, L. (2021). Numerical study on rotating detonation stability in two-phase kerosene-air mixture. Combustion and Flame, 231, 111484.

[12] Le, J., Yang, S., Liu, W., & Xing, J. (2012). Massively parallel simulations of kerosene-fueled model scramjet. In AIAA/CIRA 13th International Space Planes and Hypersonics Systems and Technologies Conference (p. 3318).

[13] Zheng, Z. H., & Le, J. L. (2005). Massively parallel computation of three-dimensional scramjet combustor. In Shock Waves: Proceedings of the 24th International Symposium on Shock Waves Beijing, China July 11–16, 2004 (pp. 897-902). Springer Berlin Heidelberg.

[14] Xiao, B., Xing, J., Tian, Y., & Wang, X. (2015). Experimental and numerical investigations of combustion mode transition in a direct–connect scramjet combustor. Aerospace Science and Technology, 46, 331-338.

[15] Lee, J. H., Knystautas, R., & Chan, C. K. (1985, January). Turbulent flame propagation in obstacle-filled tubes. In Symposium (International) on Combustion (Vol. 20, No. 1, pp. 1663-1672). Elsevier.

[16] Teodorczyk, A., Lee, J. H. S., & Knystautas, R. (1989, January). Propagation mechanism of quasi-detonations. In Symposium (International) on Combustion (Vol. 22, No. 1, pp. 1723-1731). Elsevier.

[17] Chan, C. K., & Greig, D. R. (1989, January). The structures of fast deflagrations and quasi-detonations. In Symposium (International) on Combustion (Vol. 22, No. 1, pp. 1733-1739). Elsevier.